J Inorg Organomet Polym (2013) 23:907–916
DOI 10.1007/s10904-013-9863-4

Magnetically Separable Fe_3O_4 Nanoparticles-Decorated Reduced Graphene Oxide Nanocomposite for Catalytic Wet Hydrogen Peroxide Oxidation

Wei Liu · Jing Qian · Kun Wang · Hui Xu · Ding Jiang · Qian Liu · Xingwang Yang · Huaming Li

Received: 27 February 2013 / Accepted: 8 April 2013 / Published online: 24 April 2013

Abstract Fe_3O_4 nanoparticles-decorated reduced graphene oxide magnetic nanocomposites (Fe_3O_4/rGO NCs) were prepared by a facile one-step strategy, and further used as heterogeneous Fenton-like catalysts for catalytic wet hydrogen peroxide oxidation (CWHPO) of methylene blue (MB) at 25 °C and atmospheric pressure. The effects of variables such as the Fe_3O_4/rGO with the mass ratio of rGO, initial pH, MB concentration and H_2O_2 dosage were investigated. The Fe_3O_4/rGO NCs with rGO mass ratio of 10.0 wt % showed the highest H_2O_2-activating ability, which was six-fold than that of pure Fe_3O_4 nanoparticles (NPs). The resulting catalysts demonstrated high catalytic activity in a broad operation pH range from 5 to 9, and still retained 90.5 % catalytic activity after reuse in five cycles. Taking advantage of the combined benefits of rGO and magnetic Fe_3O_4 NPs, these Fe_3O_4/rGO NCs were confirmed as an efficient heterogeneous Fenton-like catalyst for CWHPO to treat organic pollutants. And a reasonable catalytic mechanism of Fe_3O_4/rGO NCs was proposed to interpret the degradation process.

Keywords Catalytic wet hydrogen peroxide oxidation · Fe_3O_4 nanoparticles · Reduced graphene oxide · Magnetically separable catalyst · Methylene blue

The submission is intended for the 2nd International Congress on Advanced Materials.

W. Liu · J. Qian · K. Wang (✉) · H. Xu · D. Jiang · Q. Liu · X. Yang · H. Li
Key Laboratory of Modern Agriculture Equipment and Technology, School of Chemistry and Chemical Engineering, Jiangsu University, Zhenjiang 212013, People's Republic of China
e-mail: wangkun@ujs.edu.cn

1 Introduction

With large-scale production and extensive application of synthetic dyes, large quantities of dye wastewater have produced adverse effects on the environment, aquatic life and human health due to their non-biodegradability, toxicity, potential carcinogenic and mutagenic nature [1, 2]. For this reason, many wastewater treatment technologies including physicochemical and chemical methods, advanced oxidation processes, and etc., have been extensively developed during the past decades [3]. Hereinto, catalytic wet hydrogen peroxide oxidation (CWHPO) is considered as one of the most effective, simple and economical technologies [4–7]. On one hand, that is because organic pollutants can be oxidized to water, carbon dioxide, and other harmless small molecules by CWHPO process. On the other hand, that is due to CWHPO process can be operated under ambient conditions without restrictions, including high operation costs and/or the need of special equipment.

As a typical case of CWHPO, the applications of the classic Fenton/Fenton-like process have been extensive researched, which involves a strong reactive mixture of H_2O_2 and ferrous (Fe^{2+}) and/or ferric (Fe^{3+}) ions [8]. In order to overcome the well-known drawbacks of this process, namely the need to recover iron after the treatment and the need to operate in a limited pH range (2.0–4.0), various heterogeneous Fenton/Fenton-like catalysts have been already designed and prepared by combining iron/iron-containing compounds with suitable catalyst carrier or promoter, such as carbon materials [9, 10], silica, zeolites, clays [11, 12] and etc. All these resulting heterogeneous catalysts have been proved to effectively activate H_2O_2 for the oxidative degradation of various organic contaminants under ambient conditions, and more convenient than

homogeneous catalysis because its recyclability and insolubility in the reaction medium makes the separation of the product and un-reacted reactant easy.

Recent progresses in advanced nanoscience and nanotechnology have presented the opportunity to design a series of novel nano-fabrication materials or composite material for different applications [13–16]. During the recent years, graphene has been regarded as an ideal high performance candidate for catalyst carrier or promoter, due to its unique atom-thick two-dimensional structure, excellent transparency, high specific surface area, superior electron mobility, high chemical stability, and etc. [15, 16]. Especially, various graphene-based semiconductor nanocomposites coupling with suitable semiconductor nanocrystals have been prepared and further applied in the photocatalysis field including nonselective processes for degradation of pollutants [17], selective transformations for organic synthesis [18] and water splitting to clean hydrogen energy [19]. And many previous researches [20, 21] have proved the photocatalytic efficiency of various graphene-based semiconductor nanocomposites have been significantly improved after the introduction of graphene sheets. On the other hand, some graphene-based semiconductor nanocomposites with high loading capacity, especially of graphene-based Fe_3O_4 magnetic nanocomposites [22–26] have been studied as the adsorbents for dye pollutants and other hazardous substances with ease of magnetic separation. As we know, physicochemical technologies (such as adsorption, coagulation, and membrane separation) merely transferred pollutants from one medium to another, and requiring further treatment [27].

Fe_3O_4 magnetic nanoparticles (NPs) could be used for CWHPO to induce the degradation of organic pollutants due to its intrinsic enzyme mimetic activity similar to natural horseradish peroxidase [28–31] and other characters such as easy preparation, relatively low cost, and friendly environment [32]. To the best of our knowledge, there has not yet been reported on the use of the graphene-based semiconductor nanocomposites as heterogeneous catalysts in the field of CWHPO technology. Herein, a facile one step strategy toward the synthesis of the Fe_3O_4/rGO NCs was developed by chemical coprecipitation of Fe^{2+} and Fe^{3+} in alkaline solution and in situ reduction of GO into rGO by hydrazine, and assessed for catalytic activity. To evaluate the catalytic activity of the synthetic Fe_3O_4/rGO NCs magnetic material, methylene blue (MB) was selected as the model dye, which is an important member of the thiazine class of dyes, and has been extensively used as a colorant for paper, cotton, silk and leather [33]. The effects of variables such as the catalysts with mass ratio of rGO, initial pH, MB concentration and H_2O_2 dosage were investigated in detail. In this way, Fe_3O_4/rGO NCs were confirmed as a new heterogeneous Fenton-like catalyst for CWHPO to treat dye pollutants with ease of magnetic separation.

2 Experimental Section

2.1 Materials and Reagents

Graphite was purchased from Qingdao Tianhe Graphite Co., Ltd. Hydrazine hydrate (80 %),ferric chloride ($FeCl_3$), ferrous chloride ($FeCl_2$), hydrogen peroxide (30 %), MB, potassium titanium oxalate ($K_2TiO(C_2O_4)_2$), and tert-butanol were purchased from Sinopharm Chemical Reagent Co., Ltd. All the reagents were used as purchased without further purification. Double-distilled water was used throughout the study.

2.2 Preparation of Fe_3O_4/rGO

GO was synthesized from natural graphite powder according to a modified Hummers method [34]. To obtain the Fe_3O_4/rGO NCs, an aqueous solution (100 mL) of $FeCl_3$ (0.03 M) and $FeCl_2$ (0.02 M) were added to the as-prepared GO suspension solution (0.5 mg mL^{-1}, 100 mL) under magnetic stirring, and the mixture was stirred for 12 h to complete ion exchange in a nitrogen atmosphere. Then, NaOH aqueous solution (6 M) was used as precipitant and added dropwise to above mixture to achieve a pH value of 10, followed by vigorous stirring for a further 1.5 h under the protection of nitrogen at 90 °C. Subsequently, hydrazine hydrate (1 mL), as a reductant, was added and stirred for another 4 h at 90 °C. The resulting solid products were isolated from the mixture in the magnetic field and washed thoroughly with water and ethanol. Finally, the products were dried under vacuum at 50 °C for 24 h, thus, Fe_3O_4/rGO NCs were successfully obtained. For comparison, Fe_3O_4 NPs and Fe_3O_4/rGO NCs with different mass ratio of rGO were synthesized via a similar procedure.

2.3 Characterization

Fourier transform infrared (FT-IR) spectra were collected on a Nicolet Nexus 470 FT-IR spectrophotometer (Thermo Nicolet, USA). Raman spectra were recorded on a RM 2000 microscopic confocal Raman spectrometer (Renishaw in via Plus, England). The morphology of the as-prepared products was studied by using transmission electron microscopy (TEM, JEOL 2100, Japan) operated at 200 kV. X-ray diffraction (XRD) spectra were obtained using a Bruker D8 ADVANCE diffractometer (Germany) with Cu Kα ($\lambda = 1.5406$ Å) radiation. Magnetic measurements were carried out using a vibrating sample magnetometer

(VSM, LDJ9600, USA). The UV–Vis diffuse reflectance spectra of the sample were measured on a Perkin-Elmer Lambda 18 UV–Vis–NIR spectrometer (USA). The concentrations of MB were determined spectrophotometrically by the UV–Vis spectrophotometer spectrometer (Perkin-Elmer, USA). To obtain the point of zero charge (pH_{pzc}), zeta potential of samples were measured in a Malvern Nano-ZS apparatus (England). The amount of suspended sample used in each determination was approximately 100 mg L^{-1}. The pH was adjusted with HCl and NaOH. Suspensions were stabilised 24 h before measurements.

2.4 CWHPO Test

The CWHPO performance of catalyst was carried out in a 200 mL cylindrical opaque jacketed glass reactor with mechanical stirring at 25 °C. In a typical run, 30 mg Fe_3O_4/rGO NCs were added into 100 mL aqueous solution of MB (10 mg L^{-1}) and the suspension was stirred for 30 min to achieve adsorption equilibrium (Adsorption, −30–0 min). Then, the degradation reaction (Reaction, 0–120 min) was initiated (0 min) by adding H_2O_2 (60 mM) at neutral pH. At given time intervals, 4 mL solution was taken out and the residual catalysts were removed by a permanent magnet. The solution concentration of dye was determined using a UV–Vis spectrophotometer at 664 nm. The concentration of MB is proportional to absorbance of MB, so the degradation efficiency of MB can be calculated by the following equation:

$$\text{Degradation efficiency} = \left(1 - \frac{C_t}{C_0}\right) \times 100\% = \left(1 - \frac{A_t}{A_0}\right) \times 100\% \quad (1)$$

Where C_0, C_t, and A_0, A_t are the concentration and absorbance of MB when reaction time is 0 and t, respectively. In the repetition use experiment of the catalyst, Fe_3O_4/rGO NCs were isolated by a permanent magnet, washed with water several times and then dried under vacuum at 50 °C over 24 h for the next use.

Total organic carbon (TOC) was determined by TOC analyzer (TOC, Analyti kjena AG, Germany) after filtration through 0.45 μm membrane filter. Normalized TOC concentration (TOC removal) was used to quantitatively characterize the total MB mineralization. This parameter is defined as follows:

$$\text{TOC removal} = \left(1 - \frac{\text{TOC}_t}{\text{TOC}_0}\right) \times 100\% \quad (2)$$

where TOC_t and TOC_0 are the TOC values at reaction time t and 0, respectively.

To test the leaching of iron from Fe_3O_4/rGO NCs into aqueous solution, the supernatants of reaction solutions after 30 min reaction at pH 5–9 were acidized with nitric acid, and iron concentrations were investigated using atomic absorption spectrophotometry (AAS, TAS-986 Purkinje General, China).

The variation of H_2O_2 concentration during reaction was analyzed using a UV–Vis spectrophotometer at 405 nm after complexation with Titanium salt [10].

3 Results and Discussion

3.1 Characterization of the As-prepared Fe_3O_4/rGO

TEM images of Fe_3O_4 NPs and Fe_3O_4/rGO NCs were shown in Fig. 1. Compared with Fe_3O_4 NPs (Fig. 1a), with the support of rGO, Fe_3O_4 NPs on the surface of the rGO sheet (Fig. 1b) were dispersed well without apparent exfoliation and aggregation. The FT-IR and Raman spectrum of GO and Fe_3O_4/rGO NCs were shown in Fig. 2a, b, respectively. Compared with GO (Fig. 2a, curve *a*), the absorption due to the C = O group (1,734 cm^{-1}) was absent and the absorption at 1,221 and 1,400 cm^{-1} were decreased in the spectrum of Fe_3O_4/rGO NCs (Fig. 2a, curve *b*), indicating that the reduction of GO to rGO by hydrazine hydrate was completed. Moreover, an additional peak near 580 cm^{-1} could be ascribed to the lattice absorption of Fe_3O_4 NPs. In Raman spectra, the D band and G band of Fe_3O_4/rGO NCs (Fig. 2b, curve *d*)

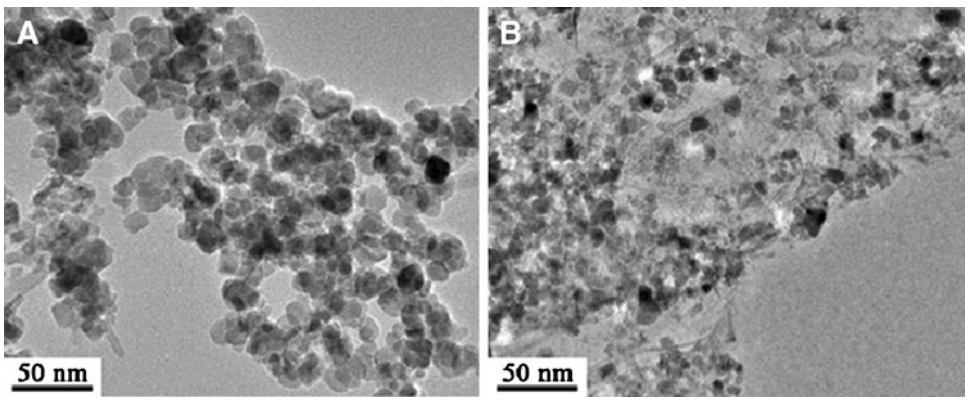

Fig. 1 TEM images of **a** Fe_3O_4 NPs and **b** Fe_3O_4/rGO NCs

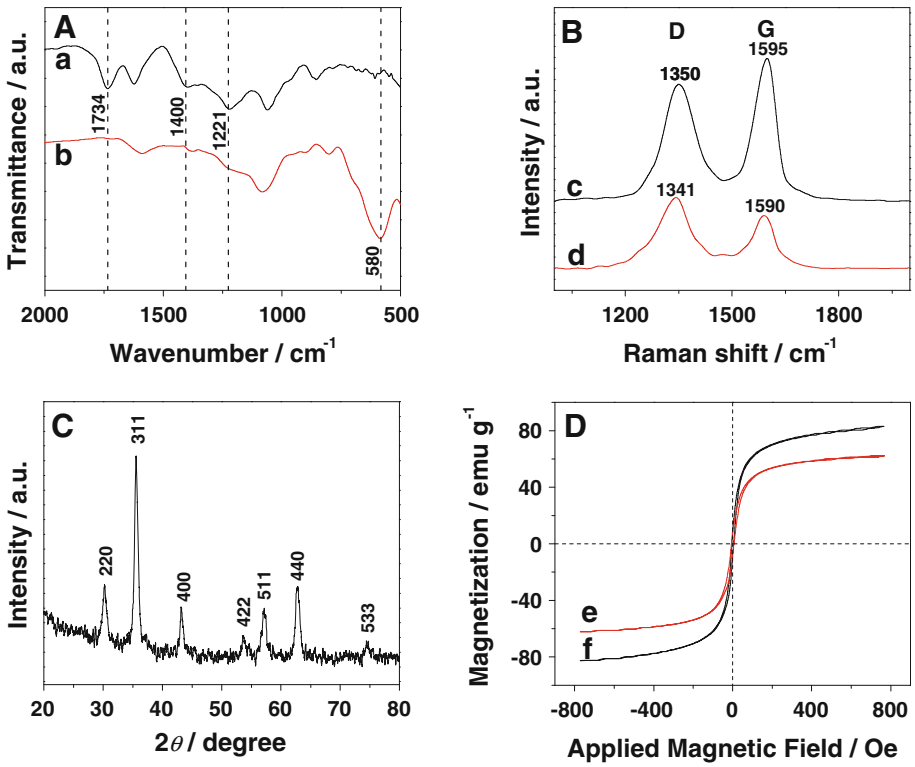

Fig. 2 **a** IR spectra for (*a*) GO and (*b*) Fe_3O_4/rGO NCs. **b** Raman spectra of (*c*) GO and (*d*) Fe_3O_4/rGO NCs. **c** XRD pattern of Fe_3O_4/rGO NCs. **d** VSM magnetization curves of synthetic (*e*) Fe_3O_4/rGO NCs and (*f*) Fe_3O_4 NPs

at 1,341 and 1,590 cm^{-1} were low ever than that of GO (Fig. 2b, curve *c*) at 1,350 and 1,595 cm^{-1}, respectively. And the D/G intensity ratio (I_D/I_G) of Fe_3O_4/rGO NCs (1.33) was much higher than that of GO (0.84). All these data indicated that the reduction of GO by hydrazine through chemical reduction. XRD characterization of Fe_3O_4/rGO NCs was conducted, which was shown in Fig. 2c. All the reflection peaks can be indexed as cubic magnetite (JCPDS No. 19-0629) [23], which suggested that the magnetite Fe_3O_4 was exclusively formed during the process of reducing GO to rGO by hydrazine hydrate.

The magnetic characterization of Fe_3O_4/rGO NCs (curve *e*) and Fe_3O_4 NPs (curve *f*) were performed by VSM at 25 °C (Fig. 2d). The M–H loops of Fe_3O_4/rGO NCs showed a non-linear and reversible behavior with an almost immeasurable magnetic hysteresis loop (nearly zero coercivity and nearly no remanence effect) when the applied magnetic field was removed, which was consistent with a super paramagnetic character [35]. The saturation magnetization of Fe_3O_4/rGO NCs was 61.9 emu g^{-1}, which was lower than that of Fe_3O_4 NPs. The saturation magnetization value of Fe_3O_4/rGO NCs was much larger than 16.3 emu g^{-1}, which was enough for magnetic separation from solution with a magnet [29].

3.2 The CWHPO Performance of Fe_3O_4/rGO NCs Catalyst

The CWHPO performance of Fe_3O_4/rGO NCs, used as heterogeneous catalyst, was evaluated by the oxidation of MB with H_2O_2 in aqueous solution. The time profiles of MB degradation under various reaction conditions were displayed in Fig. 3a. When H_2O_2 was added only, MB was hardly decayed in 120 min (Fig. 3a, curve *a*). When adding H_2O_2 to the MB solution with Fe_3O_4 NPs as a catalyst, 17.7 % of MB was degraded in the same time (Fig. 3a, curve *b*). When rGO (3 mg, 10.0 wt % rGO in Fe_3O_4/rGO NCs) was used as a catalyst, 20.5 % of MB was adsorbed by rGO in 30 min before adding H_2O_2, then 24.5 % of MB was removed after 120 min reaction with H_2O_2 presence (Fig. 3a, curve *c*). This indicates that graphene, as other carbon materials, shows catalytic activity in CWHPO process [36, 37]. The high adsorption performance of the rGO for MB removal could be attributed to the following two factors [34]: (i) the electrostatic attraction between the negatively charged surface oxygen-containing groups and cationic MB; (ii) the π–π interactions between the MB molecules and the aromatic rings of rGO. When only adding Fe_3O_4/rGO NCs to the MB solution without H_2O_2 presence, 30.2 % of MB was removed because of adsorption (Fig. 3a, curve *d*). However, remarkable MB degradation occurred in Fe_3O_4/rGO NCs suspension with H_2O_2 presence and about 98.6 % of MB was degraded in the same time (Fig. 3a, curve *e*), which was about six folds than that of Fe_3O_4 NPs as the catalyst under the same condition. And the temporal evolutions of UV–Vis spectra taking place during the degradation of MB by Fe_3O_4/rGO NCs with H_2O_2 presence were shown in Fig. 3b. The major absorption peak of MB at 664 nm

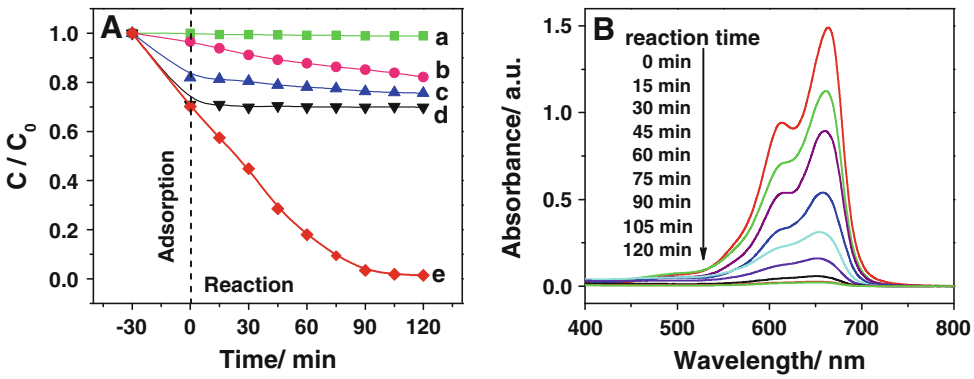

Fig. 3 **a** Degradation efficiency in different system under optimized conditions: (*a*) H_2O_2, (*b*) Fe_3O_4 NPs + H_2O_2, (*c*) rGO + H_2O_2, (*d*) Fe_3O_4/rGO NCs and (*e*) Fe_3O_4/rGO NCs + H_2O_2 **b** Time-dependent absorption spectrum of MB solution in (*e*) condition

gradually decreased in 120 min and no new peaks were observed during the degradation reaction. These results indicated that MB was successfully degraded.

3.2.1 *Influence of Mass Ratio of rGO in Fe_3O_4/rGO NCs*

To further study the synergetic effect of rGO and Fe_3O_4 NPs in CWHPO process, a series of Fe_3O_4/rGO NCs with different mass ratio of rGO were synthesized and tested (Fig. 4a). The catalytic activity was gradually enhanced with the amount of rGO increasing. When the ratio of rGO got to 10.0 wt %, the as-prepared Fe_3O_4/rGO NCs had the optimal catalytic activity and 98.6 % MB could be removed (Fig. 4a). It remained higher than that of Fe_3O_4 NPs, though the degradation efficiency decreased with the further increase of rGO. That was due to the fact that the decrease of Fe_3O_4 NPs supported on rGO sheets lead to the reduction of radicals, which were generated by the reaction of Fe_3O_4 and H_2O_2. In order to achieve the best catalytic activity, the mass ratio of rGO in the experiment was chosen as 10.0 wt %.

3.2.2 *Influence of pH*

To investigate the effect of pH on the degradation performance of Fe_3O_4/rGO NCs, experiments were carried out at different pH values from 3 to 11 (Fig. 4b). It was observed that the degradation efficiency was satisfactory in a wide pH range of 5–9, while the optimal pH value of 7 was obtained with a degradation efficiency as high as 98.6 %. Furthermore, when the initial pH of MB solution was extremely acidic (pH = 3) or alkaline (pH = 11), the degradation efficiency of MB was considerably low. The rGO sheets were negatively charged in solution due to the presence of the oxygen-containing groups [25], and cationic MB molecule could absorb on the surface of the Fe_3O_4/rGO NCs by electrostatic attraction. When the solution pH is higher than the pH_{pzc}, the surface of the adsorbent is negatively charged, favouring the adsorption of cationic species [37]. The measured pH_{pzc} value of Fe_3O_4/rGO NCs was 5.9. Thus, the surface of Fe_3O_4/rGO NCs was negatively charged, when the pH vaule of reaction solution was higher than 5.9.

Under acidic conditions (pH = 3), the surface of the Fe_3O_4/rGO NCs was positively charged, so the adsorption of MB molecule decreased. As a result, the degradation efficiency of MB reduced to 66.5 %. Under alkaline (pH = 11) conditions, the surface of the Fe_3O_4/rGO NCs was negatively charged, favouring the adsorption of cationic MB molecule. However, the degradation efficiency of MB considerably reduced to 65.0 %, which was caused by two reasons. Firstly, H_2O_2 is not stable in alkaline solution, and could be decomposed to produce H_2O and O_2 as shown in Eq. 3 [29]. Secondly, a high-valent iron species ($\equiv Fe^{IV} = O$), which are less reactive than HO· radicals, might be formed under alkaline conditions according to Eq. 4 [38].

$$2H_2O_2 \rightarrow 2H_2O + O_2 \quad (3)$$

$$\equiv Fe^{II} + H_2O_2 \rightarrow \equiv Fe^{IV} = O + H_2O \quad (4)$$

Thus, the wide operation pH (pH = 5–9) range was due to the Fe_3O_4/rGO NCs combined with both features of Fe_3O_4 NPs and rGO. Under acid condition, the reaction of radicals generation by Fe_3O_4 and H_2O_2 was more effective. The higher pH value was the stronger adsorptive capacity of Fe_3O_4/rGO NCs was, which made the reaction of radicals and MB more effective.

3.2.3 *Influence of Initial MB Concentration*

The effect of initial MB concentrations on the degradation performance of Fe_3O_4/rGO NCs was investigated between 10 and 50 mg L^{-1} MB solutions (Fig. 4c). The degradation rate was decreased slightly by the increasing initial MB concentrations to 20 mg L^{-1} (Fig. 4c, curve *b*). Under higher initial MB concentrations the degradation rate was decreased remarkably (Fig. 4c, curve *c*–*e*). The increase in dye concentration enhanced the adsorption of dye molecules on the catalyst surface, limiting the generation of HO· radicals, and resulting the degradation rate decreased [5].

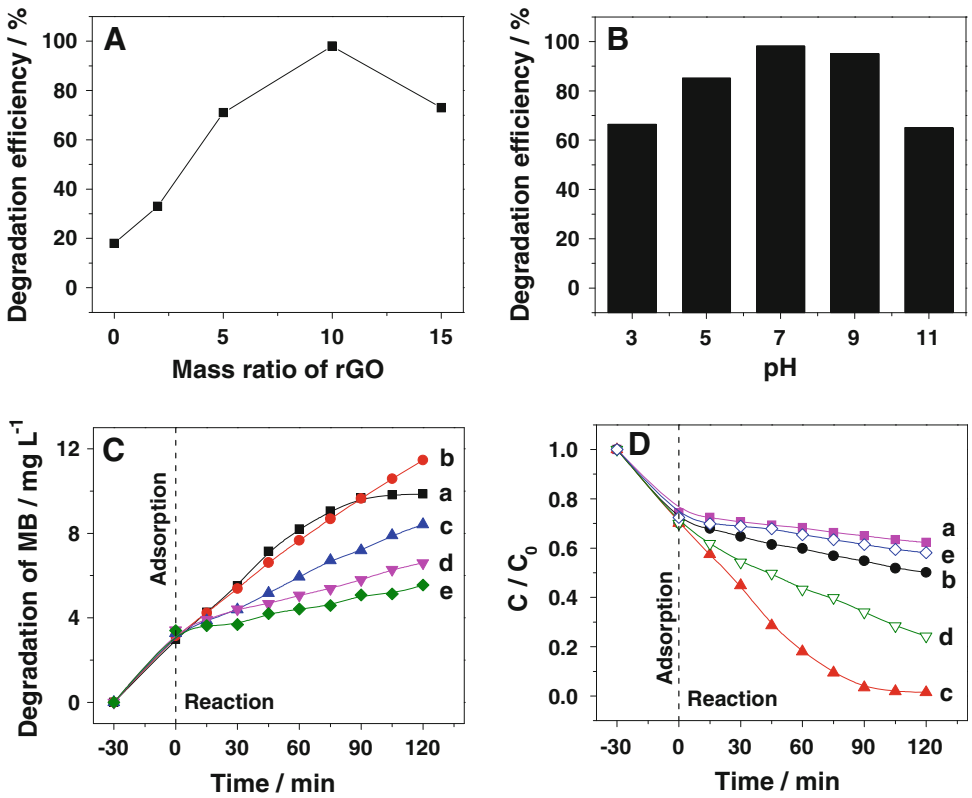

Fig. 4 **a** The dependence of the mass ratio of rGO in Fe_3O_4/rGO NCs on MB degradation efficiency; **b** Effect of pH on the catalytic degradation of MB; **c** Effect of initial MB concentration of (*a*) 10, (*b*) 20, (*c*) 30, (*d*) 40 and (*e*) 50 mg L^{-1} on the degradation process; and **d** Effect of H_2O_2 concentration of (*a*) 15, (*b*) 30, (*c*) 60, (*d*) 120 and (*e*) 120 mM on the catalytic degradation of MB

Hence, oxidation process required more catalyst loading and longer reaction time for higher dye concentrations.

3.2.4 *Influence of H_2O_2 Concentration*

The effect of initial H_2O_2 concentrations on the degradation performance of Fe_3O_4/rGO NCs was studied and shown in Fig. 4. The degradation efficiency of MB increased with the increasing of H_2O_2 concentration. When the H_2O_2 concentration was 15, 30 and 60 mM, the degradation efficiency of MB were 37.8 %, 49.8 % and 98.6 %, respectively (Fig. 4d, curve *a–c*). Because at low concentration, H_2O_2 could not generate enough radicals to degrade MB and the oxidation rate was logically slow. When the initial H_2O_2 concentration was improved to 120 mM, the degradation efficiency of MB declined to 75.7 % (Fig. 4d, curve *d*). With increasing the concentration of H_2O_2, the degradation efficiency of MB continued to toward the downward trend and the degradation efficiency as low as 41.8 % was obtained with a H_2O_2 concentration of 240 mM (Fig. 4d, curve *e*). Addition of the excess of H_2O_2, the scavenging of HO· radicals would occur, which could be expressed by the reaction Eqs. 5 and 6 [39]. Therefore, to achieve high degradation efficiency of MB in shorter treatment time, an optimal concentration of H_2O_2 was selected to be 0.06 M in the present work.

$$H_2O_2 + HO\cdot \rightarrow H_2O + HO_2\cdot \quad (5)$$

$$HO_2\cdot + HO\cdot \rightarrow H_2O + O_2 \quad (6)$$

3.2.5 *Mineralization of MB and H_2O_2 Decomposition*

The activity of Fe_3O_4/rGO NCs for degradation and TOC removal in the oxidation of MB and for H_2O_2 decomposition were shown in Fig. 5a. The maximum of TOC removal was 28.5 % while that of MB removal was nearly 100 % after 120 min reaction. During 120 min reaction about 4.77 mM H_2O_2 was consumed (Fig. 5b).

3.3 Degradation Kinetics and Possible Catalytic Mechanism

Kinetics was studied for this CWHPO process, where used Fe_3O_4/rGO NCs as heterogeneous catalyst and MB as model dye. The parameters k and (C/C_0) of MB degradation on Fe_3O_4/rGO NCs (Fig. 6b) were calculated. As shown in Table 1, the data of without and with tert-butanol both showed an excellent linear correlation, and the linear correlation values (R^2) were 0.9958 and 0.9987, respectively, suggesting that the degradation reaction follows the zero-order kinetics and can be expressed as:

$$C_0 - C_t = kt \quad (7)$$

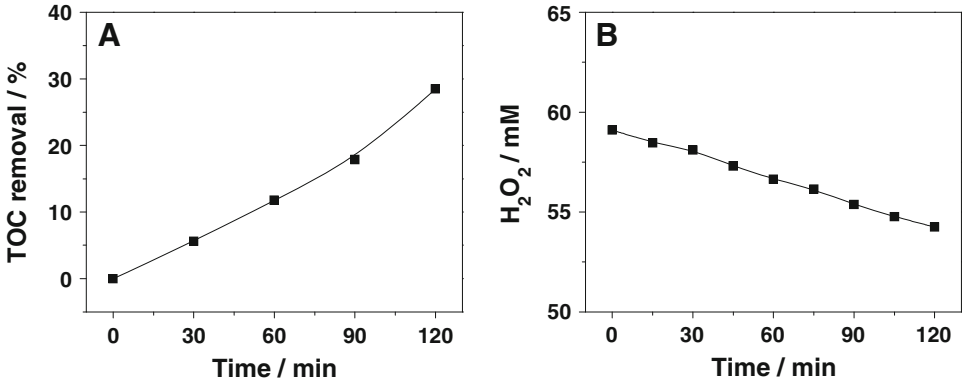

Fig. 5 **a** TOC removal of MB and **b** H_2O_2 decomposition under optimized conditions

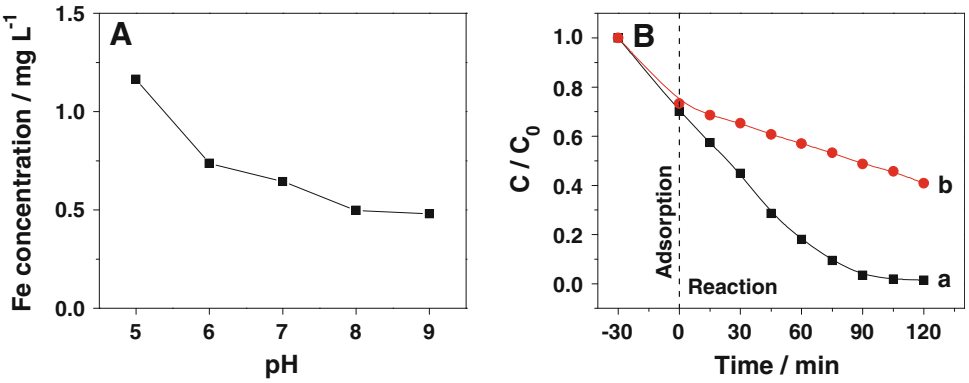

Fig. 6 **a** Iron concentration in the supernatants of reaction solution at different pH after 30 min reaction; **b** Effect of the absence (*a*) and presence (*b*) of tert-butanol (0.3 mM) on MB degradation efficiency under optimized conditions

where C_0 and C_t are the MB concentrations (mmol L^{-1}) at the initial time and reaction time *t*, k is zero-order apparent rate constant (mmol L^{-1} min^{-1}). With adding the tert-butanol in the reaction system, the zero-order kinetic rate constant k decreases from 0.00888 to 0.0026 mmol L^{-1} min^{-1}. In contrast, the plots of first-order kinetics give poor linear correlation values. However, for MB degradation on Fe_3O_4/rGO NCs, the fit of the data deviated from the straight line after 60 min reaction. That was due to the concentration of MB was lower than that for the surface of Fe_3O_4/rGO NCs to be saturated with adsorbed MB, resulting the reaction rate decreased gradually during the degradation [40].

When Fe_3O_4 NPs are used as heterogeneous catalyst in CWHPO process, there are many types of active species, such as iron cations on the surface [28, 29], leaching of filterable Fe and iron ions [41]. To test the leaching of iron from Fe_3O_4/rGO NCs into aqueous solution, iron concentrations were investigated using AAS. As can be seen from Fig. 6a, the iron concentrations leaching into the reaction solutions were decreased by increasing pH value. At pH 5 the maximum iron concentration was 1.16 mg L^{-1}. Thus, the homogeneous degradation efficiency of MB was studied by using ferrous (1.16 mg L^{-1}) as the catalyst under the same conditions. However, under this condition MB was hardly decayed in 120 min. Thus, the possibly leached Fe^{2+} ions did not show catalytic activity, and homogeneous degradation efficiency could be ignored. And the reaction could be considered as the heterogeneous Fenton reaction, which degraded organic compounds on the catalyst surface, controlled the efficiency of the process [39], resulting from the fact that radicals were extraordinarily reactive species and short-lived [5].

To our knowledge, Fe_3O_4 NPs can be used as heterogeneous catalyst in CWHPO process, due to the fact that Fe_3O_4 NPs can directly activate H_2O_2 to form reactive oxygen species (ROS), such as hydroxyl (HO·), superoxide (O_2^{-}·), and perhydroxyl (HO_2·). The possible generation process of ROS using Fe_3O_4/rGO NCs as catalyst was proposed and described as following processes [29, 30, 42]:

$$\equiv Fe^{II} + H_2O_2 \rightarrow \equiv Fe^{III} + HO\cdot + OH^- \quad (8)$$

$$\equiv Fe^{III} + H_2O_2 \rightarrow \equiv Fe^{II} + HO_2\cdot + H^+ \quad (9)$$

$$\equiv Fe^{III} + HO_2\cdot \rightarrow \equiv Fe^{II} + O_2 + H^+ \quad (10)$$

$$MB + HO\cdot \rightarrow \cdots \rightarrow \text{products} \quad (11)$$

when excessive H_2O_2 was added into the reaction system, a redox process Fe(II) ↔ Fe(III) on the surface of Fe_3O_4/rGO NCs took place to produce HO· and O_2^{-}·/HO_2· radicals and the generated radicals were capable of degrading MB into organic compounds or small organic molecules [29, 38]. To gain further insights into the existence of

Table 1 The rate constant for the degradation of MB through CWHPO reaction catalyzed by Fe_3O_4/rGO NCs without or with tert-butanol (0.3 mM) under optimized conditions

Experiment condition	Zero-order		First-order		Applied stage
	k (mmol L^{-1} min^{-1})	R^2	k (min^{-1})	R^2	
Fe_3O_4/rGO NCs	0.00888	0.9958	0.02281	0.95612	Before 60 min
Fe_3O_4/rGO NCs + tert-butanol	0.0026	0.9987	0.0047	0.991	All

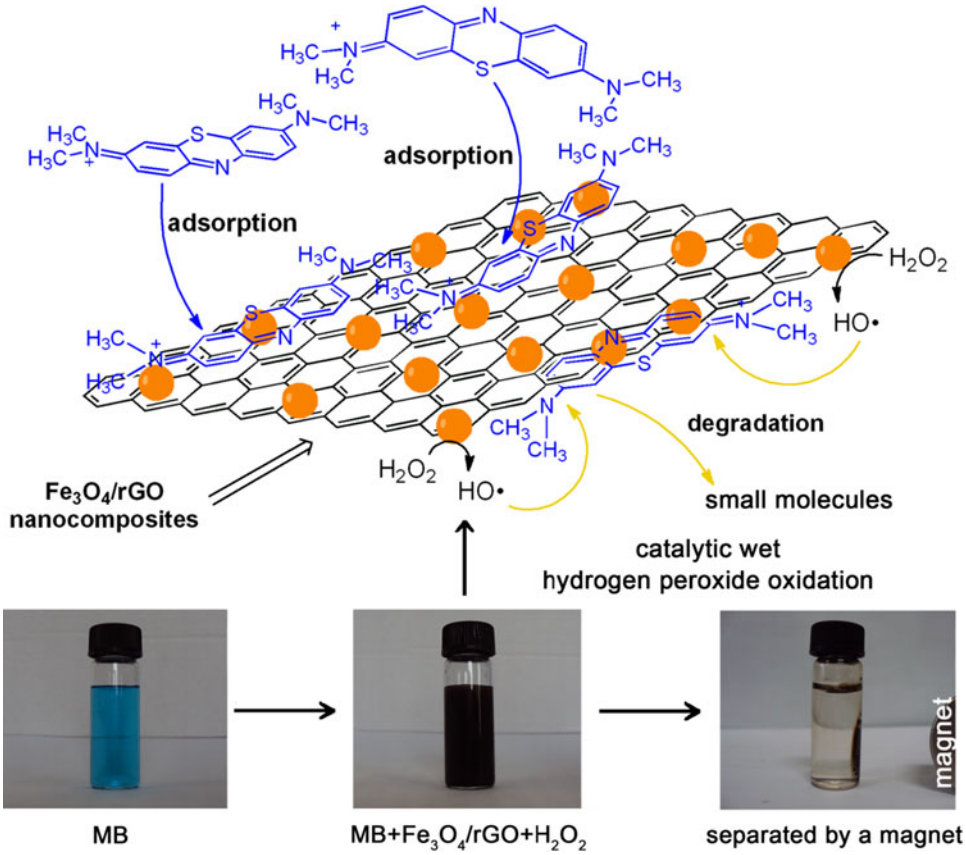

Scheme 1 Schematic structure of Fe_3O_4/rGO NCs and tentative processes of degradation of MB. Where the inset shows the photographs of Fe_3O_4/rGO NCs dispersed in MNCs B and H_2O_2 solution and magnetic separation by a permanent magnet after degradation of MB

hydroxyl free radical, tert-butanol, a strong radical scavenger [29], was added before reaction (Fig. 6b). The degradation of MB was greatly suppressed with the addition of 0.3 mM tert-butanol (Fig. 6b, curve *b*), indicating that the hydroxyl free radicals were mainly responsible for the degradation of MB.

Coupled with Eqs. 8–11 and the control experiment results, we may demonstrate the main route of MB degradation by H_2O_2 with Fe_3O_4/rGO NCs as heterogeneous catalyst, which was shown in scheme 1. H_2O_2 was activated to generate HO· radicals on the surface of Fe_3O_4 NPs, and the radicals diffused through solution and attacked MB molecules, which were adsorbed on the surface of Fe_3O_4/rGO NCs. The MB molecules were destroyed by the HO· radicals and finally produced harmless organic compounds or small organic molecules. With the degradation of MB, the adsorption equilibrium broke and more MB could transfer from solution to the surface of Fe_3O_4/rGO NCs, forming a cyclic process. After the degradation process, Fe_3O_4/rGO NCs could be easily manipulated by a permanent magnet for reusing. Further experimental and theoretical investigations are underway in our laboratory to make the proposed approach as a new platform for dye decontamination and to receive a clearer insight to the related mechanism.

3.4 Regeneration and Reuse of Fe_3O_4/rGO

The regeneration and reuse of the catalyst is one of the important issues in practical operation for the ecological and economic demands. The Fe_3O_4/rGO NCs catalyst could be separated easily from the reaction system by a permanent magnet and successfully reused. And the reusability of Fe_3O_4/rGO NCs was examined under the above optimized

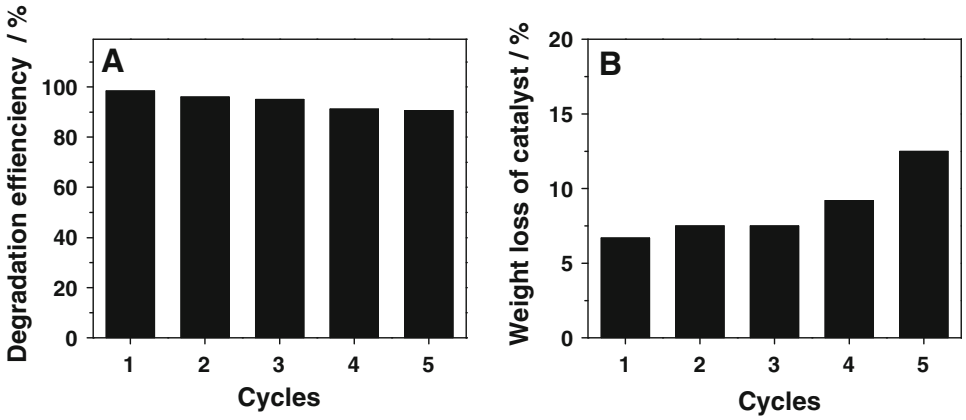

Fig. 7 **a** Degradation efficiency of MB under optimized conditions in recycles experiment; **b** weight loss of catalyst after recycles experiment

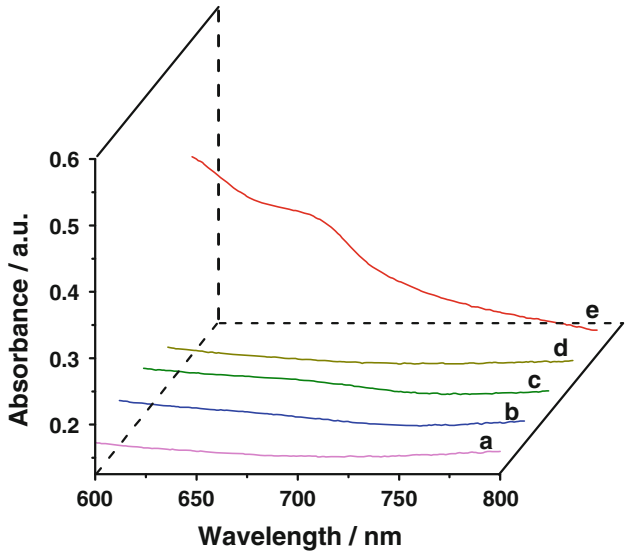

Fig. 8 Diffuse reflectance UV–Vis spectra of (*a*) Fe_3O_4/rGO NCs, Fe_3O_4/rGO NCs separated from the reacting system at (*b*) 30, (*c*) 75 and (*d*) 120 min, and (*e*) MB powder

conditions. As shown in Fig. 7a, the degradation efficiency of MB was still over 90 % after five cycles. And the weight loss of Fe_3O_4/rGO after five cycles was 12.5 % (Fig. 7b). Thus, the slightly lower of degradation efficiency may due to the loss of catalyst in the recovery and washing process.

The stability of Fe_3O_4/rGO NCs catalyst in the reaction medium was also investigated through iron leaching tests. After catalysts removed by a magnet from the reaction solution, iron concentrations of the reaction solution before and after filtration through 0.45 μm membrane filters were 0.22 and < 0.1 mg L^{-1}. These results suggest that the as-prepared catalyst had good reusability and stability and the leaching of iron in this system might not cause metal pollution in the water.

The UV–Vis diffuse reflectance absorption spectra changes were taken to study the residual MB on Fe_3O_4/rGO NCs during the degradation process (Fig. 8). In the wavelength range from 600 to 800 nm, there was a wide peak at 660 nm obtained from the pristine MB (Fig. 8*e*), and the fresh Fe_3O_4/rGO NCs used before the degradation of MB showed no absorption in the same range (Fig. 8*a*). The catalysts obtained from the reaction of MB degradation (optimum conditions) were separated by a permanent magnet for 30, 75 and 120 min, and dried under vacuum at 50 °C for 24 h, respectively. As shown in Fig. 8*b*, due to the existance of MB, a wide peak appeared at 680 nm after 30 min of the reaction. The peak of MB reduced gradually until disappeared after 120 min of the reaction (Fig. 8*d*), resulting from the complete degradation of MB. Moreover, the UV–Vis diffuse reflectance absorption spectra of Fe_3O_4/rGO NCs after MB degradation (Fig. 8*d*) was similar to the freshly prepared Fe_3O_4/rGO NCs (Fig. 8*a*), indicating that there was no residual MB on the surface of Fe_3O_4/rGO NCs after the degradation of MB at optimum condition after 120 min.

4 Conclusion

Fe_3O_4/rGO NCs were successfully synthesized by a simple one-step solvothermal method and used as heterogeneous Fenton-like catalysts for CWHPO application. Benefiting from the combined features of magnetic Fe_3O_4 NPs and graphene, the catalytic ability of Fe_3O_4/rGO NCs was much higher than that of Fe_3O_4 NPs as the catalyst under the same condition. All these results suggested that Fe_3O_4/rGO NCs could effectively catalyze the decomposition of H_2O_2 and a possible reaction mechanism on the surface of this material was also proposed. With several advantages such as environmental benignity, wide working pH range, easy of separation, and good operational recyclability, we believe our route could provide a new platform for purification treatment for organic pollutants.

Acknowledgments The present work is supported by the National Natural Science Foundation of China (Nos. 21007021, 21177050, and 21175061), and Key Laboratory of Modern Agriculture Equipment and Technology (No. NZ201109).

References

1. C.A. Martínez-Huitle, E. Brillas, Appl. Catal. B: Environ. **87**, 105 (2009)
2. S.K. Ling, S.B. Wang, Y.L. Peng, J. Hazard. Mate. **178**, 385 (2010)
3. E. Forgacs, T. Cserháti, G. Oros, Environ. Int. **30**, 953 (2004)
4. A. Dhakshinamoorthy, S. Navalon, M. Alvaro, H. Garcia, ChemSusChem **5**, 46 (2012)
5. Y.Z. Zhan, H.L. Li, Y.L. Chen, J. Hazard. Mater. **180**, 481 (2010)
6. A.M. Cojocariu, P.H. Mutin, E. Dumitriu, A. Vioux, F. Fajula, V. Hulea, Chemosphere **77**, 1065 (2009)
7. M. Hermanek, R. Zboril, I. Medrik, J. Pechousek, C. Gregor, J. Am. Chem. Soc. **129**, 10929 (2007)
8. R.X. Huang, Z.Q. Fang, X.M. Yan, W. Cheng, Chem. Eng. J. **197**, 242 (2012)
9. A. Dhaouadi, N. Adhoum, Appl. Catal. B: Environ. **97**, 227 (2010)
10. X.B. Hu, B.Z. Liu, Y.H. Deng, H.Z. Chen, S. Luo, C. Sun, P. Yang, S.G. Yang, Appl. Catal. B: Environ. **107**, 274 (2011)
11. S. Navalon, M. Alvaro, H. Garcia, Appl. Catal. B: Environ. **1**, 99 (2010)
12. R. Prihod'ko, I. Stolyarova, G. Gunduz, O. Taran, S. Yashnik, V. Parmon, V. Goncharuk, Appl. Catal. B: Environ. **104**, 201 (2011)
13. L.F. Hu, M. Chen, X.S. Fang, L.M. Wu, Chem. Soc. Rev. **41**, 1350 (2012)
14. L.M. Dai, Acc. Chem. Res. **46**, 31 (2013)
15. C.C. Huang, C. Li, G.Q. Shi, Energy Environ. Sci. **5**, 8848 (2012)
16. X.Q. An, J.C. Yu, RSC Adv. **1**, 1426 (2011)
17. H. Zhang, X.J. Lv, Y.M. Li, Y. Wang, J.H. Li, ACS Nano **4**, 380 (2010)
18. Y.H. Zhang, Z.R. Tang, X.Z. Fu, Y.J. Xu, ACS Nano **5**, 7426 (2011)
19. Q. Li, B.D. Guo, J.G. Yu, J.R. Ran, B.H. Zhang, H.J. Yan, J.R. Gong, J. Am. Chem. Soc. **133**, 10878 (2011)
20. T.G. Xu, L.W. Zhang, H.Y. Cheng, Y.F. Zhu, Appl. Catal. B: Environ. **101**, 382 (2011)
21. X.W. Wang, H.W. Tian, Y. Yang, H. Wang, S.M. Wang, W.T. Zheng, Y.C. Liu, J. Alloy. Compd. **524**, 5 (2012)
22. G.Q. Xie, P.X. Xi, H.Y. Liu, F.J. Chen, L. Huang, Y.J. Shi, F.P. Hou, Z.Z. Zeng, C.W. Shao, J. Wang, J. Mater. Chem. **22**, 1033 (2012)
23. H. Sun, L. Cao, L. Lu, Nano Res. **4**, 550 (2011)
24. C. Wang, C. Feng, Y. Gao, X. Ma, Q. Wu, Z. Wang, Chem. Eng. J. **173**, 92 (2011)
25. L. Ai, C. Zhang, Z. Chen, J. Hazard. Mater. **192**, 1515 (2011)
26. Z.G. Geng, Y. Lin, X.X. Yu, Q.H. Shen, L. Ma, Z.Y. Li, N. Pan, X.P. Wang, J. Mater. Chem. **22**, 3527 (2012)
27. S. Perathoner, G. Centi, Top. Catal. **33**, 1 (2005)
28. L.J. Xu, J.L. Wang, Appl. Catal. B: Environ. **123–124**, 117 (2012)
29. S.X. Zhang, X.L. Zhao, H.Y. Niu, Y.L. Shi, Y.Q. Cai, G.B. Jiang, J. Hazard. Mater. **167**, 560 (2009)
30. N. Wang, L.H. Zhu, D.L. Wang, M.Q. Wang, Z.F. Lin, H.Q. Tang, Ultrason. Sonochem. **17**, 526 (2010)
31. J.B. Zhang, J. Zhuang, L.Z. Gao, Y. Zhang, N. Gu, J. Feng, D.L. Yang, J.D. Zhu, X.Y. Yan, Chemosphere **73**, 1524 (2008)
32. M.Q. Wang, N. Wang, H.Q. Tang, M.J. Cao, Y.B. She, L.H. Zhu, Catal. Sci. Technol. **2**, 187 (2012)
33. K.N. Vinod, K.N. Puttaswamy, G. Ninge, Ind. Eng. Chem. Res. **49**, 3137 (2010)
34. S. Gilje, S. Han, M. Wang, K.L. Wang, R.B. Kaner, Nano Lett. **7**, 3394 (2007)
35. H.K. He, C. Gao, ACS Appl. Mater. Interfaces **2**, 3201 (2010)
36. F. Duarte, F.J. Maldonado-Hódar, L.M. Madeira, Appl. Catal. B: Environ. **103**, 109 (2011)
37. M. Soria-Sánchez, E. Castillejos-López, A. Maroto-Valiente, M.F.R. Pereira, J.J.M. Órfão, A. Guerrero-Ruiz, Appl. Catal. B: Environ. **121–122**, 182 (2012)
38. W. Luo, L.H. Zhu, N. Wang, H.Q. Tang, M.J. Cao, Y.B. She, Environ. Sci. Technol. **44**, 1786 (2010)
39. T.D. Nguyen, N.H. Phan, M.H. Do, K.T. Ngo, J. Hazard. Mater. **185**, 653 (2011)
40. S.J. Yang, H.P. He, D.Q. Wu, D. Chen, X.L. Liang, Z.H. Qin, M.D. Fan, J.X. Zhu, P. Yuan, Appl. Catal. B: Environ. **89**, 527 (2009)
41. F.C.C. Moura, M.H. Araujo, R.C.C. Costa, J.D. Fabris, J.D. Ardisson, W.A.A. Macedo, R.M. Lago, Chemosphere **60**, 1118 (2005)
42. H.Y. Niu, D. Zhang, S.X. Zhang, X.L. Zhang, Z.F. Meng, Y.Q. Cai, J. Hazard. Mater. **190**, 559 (2011)